Deterministic and stochastic chaos characterize laboratory earthquakes

Adriano Gualandi, Davide Faranda, Chris Marone, Massimo Cocco, Gianmarco Mengaldo

Earth and Planetary Science Letters 604 (2023) 117995

Contents lists available at ScienceDirect

Earth and Planetary Science Letters

journal homepage: www.elsevier.com/locate/epsl

Deterministic and stochastic chaos characterize laboratory earthquakes

A. Gualandi [a,*], D. Faranda [b,c,d], C. Marone [e,f], M. Cocco [g], G. Mengaldo [h,i]

[a] Osservatorio Nazionale Terremoti, Istituto Nazionale di Geofisica e Vulcanologia, via di Vigna Murata 605, Rome, 00143, Italy
[b] Laboratoire des Sciences du Climat et de l'Environnement, University of Paris-Saclay, Chemin de Saint Aubin - RD 128, Gif sur Yvette, F-91191, France
[c] London Mathematical Laboratory, 8 Margravine Gardens, London, W6 8RH, UK
[d] Laboratoire de Meteorologie Dynamique, École Normale Supérieure, 24 rue Lhomond, Paris, 75005, France
[e] Dipartimento di Scienze della Terra, La Sapienza Università di Roma, Piazzale Aldo Moro 5, Rome, 00185, Italy
[f] Department of Geosciences, College of Earth and Mineral Sciences, Pennsylvania State University, 503 Deike Building, University Park, 16802, PA, USA
[g] Sezione Roma 1, Istituto Nazionale di Geofisica e Vulcanologia, via di Vigna Murata 605, Rome, 00143, Italy
[h] Department of Mechanical Engineering, College of Design and Engineering, National University of Singapore, 9 Engineering Drive 1, Block EA #07-08, Singapore, 117575, Singapore
[i] Department of Aeronautics, Imperial College London, 148A, Roderic Hill Building, South Kensington Campus, London, SW7 2AZ, United Kingdom

ARTICLE INFO

Article history:
Received 18 September 2022
Received in revised form 3 January 2023
Accepted 8 January 2023
Available online xxxx
Editor: R. Bendick

Keywords:
random attractor
stochastic differential equations
rate- and state-friction
seismic cycle

ABSTRACT

We analyze frictional motion for a laboratory fault as it passes through the stability transition from stable sliding to unstable motion. We study frictional stick-slip events, which are the lab equivalent of earthquakes, via dynamical system tools in order to retrieve information on the underlying dynamics and to assess whether there are dynamical changes associated with the transition from stable to unstable motion. We find that the seismic cycle exhibits characteristics of a low-dimensional system with average dimension similar to that of natural slow earthquakes (<5). We also investigate local properties of the attractor and find maximum instantaneous dimension $\gtrsim 10$, indicating that some regions of the phase space require a high number of degrees of freedom (dofs). Our analysis does not preclude deterministic chaos, but the lab seismic cycle is best explained by a random attractor based on rate- and state-dependent friction whose dynamics is stochastically perturbed. We find that minimal variations of 0.05% of the shear and normal stresses applied to the experimental fault influence the large-scale dynamics and the recurrence time of labquakes. While complicated motion including period doubling is observed near the stability transition, even in the fully unstable regime we do not observe truly periodic behavior. Friction's nonlinear nature amplifies small scale perturbations, reducing the predictability of the otherwise periodic macroscopic dynamics. As applied to tectonic faults, our results imply that even small stress field fluctuations ($\lesssim 150$ kPa) can induce coefficient of variations in earthquake repeat time of a few percent. Moreover, these perturbations can drive an otherwise fast-slipping fault, close to the critical stability condition, into a mixed behavior involving slow and fast ruptures.

1. Introduction

Tectonic faulting and the seismic cycle involve a complicated set of processes that are only partially understood. A number of modeling strategies have been proposed in the literature, including both high- and low-dimensional models, to mimic the seismic cycle. On one hand, high-dimensional models usually require solving a set of partial differential equations describing tectonic fault's physics (e.g., Lapusta and Liu, 2009; Bizzarri and Cocco, 2006). On the other hand, low-dimensional models approximate fault behavior under simplified conditions, commonly leading to a set of ordinary differential equations (e.g., Burridge and Knopoff, 1967; Huang and Turcotte, 1990).

Any strategy to model the seismic cycle and the full spectrum of slip modes that includes aseismic slip, slow earthquakes and elastodynamic rupture requires an understanding of fault friction. The seismic cycle involves inter-seismic periods of loading followed by failure events with fast or slow unloading. These failure events correspond to earthquakes or slow slip events (or slow earthquakes), and their behavior is known as stick-slip, because of the inter-seismic loading (stick), and the failure (slip). Within this context, laboratory experiments have played a major role for understanding earthquake physics and frictional failure, providing phenomenological laws for fault friction (Dieterich, 1979; Ruina, 1983). These phenomenological laws have been used to synthesize

* Corresponding author.
E-mail address: adriano.gualandi@ingv.it (A. Gualandi).

https://doi.org/10.1016/j.epsl.2023.117995

low-dimensional models that describe the behavior of sliding surfaces with a limited number of independent variables (i.e., degrees of freedom, dofs) (e.g., Perfettini and Avouac, 2004), and provided useful constitutive laws for high-dimensional models (e.g., Lapusta and Liu, 2009; Dal Zilio et al., 2020).

In this paper, we focus on low-dimensional models to describe a recently derived set of laboratory experiments (also referred to as laboratory earthquakes or labquakes) encompassing the full spectrum of fault slip behavior, ranging from stable creep to slow and fast stress unloading, as well as mixed behavior of both slow and fast events in the same experiment (Mele Veedu et al., 2020). We consider the widely accepted framework where friction (μ) depends on both the sliding rate (v) and a state variable (θ) that embeds memory effects and fault healing (Dieterich, 1979; Ruina, 1983; Rice and Ruina, 1983). This framework defines the so-called rate- and state-dependent friction models (briefly RSF), that have been used extensively to characterize laboratory friction experiments and tectonic faulting for a wide range of systems, including labquakes where inter-seismic loading and repeating failure events are observed (e.g., Dieterich, 1979; Ruina, 1983; Gu et al., 1984; Baumberger and Caroli, 2006; Li et al., 2011; Scholz, 2019; Leeman et al., 2016), and to simulate the seismic cycle (e.g., Lapusta and Liu, 2009; Luo and Ampuero, 2018; Dal Zilio et al., 2020).

The stick-slick behavior observed in the seismic cycle is rather complicated, and modifications to the basic RSF framework have been proposed. For example, works on friction have adopted one or more state variables (Gu et al., 1984), introduced a possible dependency of frictional state on normal stress (Linker and Dieterich, 1992), and accounted for fault zone porosity and shear localization (Marone and Kilgore, 1993; Segall and Rice, 1995), or considered temperature effects (Bizzarri and Cocco, 2006). Other works have shown that RSF parameters might vary with the slip velocity (Mair and Marone, 1999), making them additional variables or dofs of the system (Im et al., 2020). Despite these and more recent works (e.g., Perfettini and Molinari, 2017; Barbot, 2022) our understanding of the seismic cycle and the number of dofs required to describe it are still unclear.

One way to improve our understanding of fault friction and the seismic cycle is through the lenses of dynamical system theory. From this perspective, we expect a set of experimental observations provided by, e.g., laboratory earthquakes, to admit the existence of some persistent dynamics or trajectories (i.e., an attractor). If we observed such an attractor, we could, in principle, calculate useful properties such as its dimension (that is, the dimension of the system's dynamical trajectories (Theiler, 1990)) and the Lyapunov spectrum associated with the system (Wolf et al., 1985; Sano and Sawada, 1985). The *attractor dimension* is a particularly important quantity as it defines the number of variables needed to fully characterize (macroscopically) the state of the system, and consequently the number of differential equations needed to describe its dynamics (i.e., the *system dimension*). This is a critical aspect, given the ambiguity regarding the number of variables required to describe the seismic cycle.

Introducing a local concept of dimension, Faranda et al. (2017a), Gualandi et al. (2020) have shown that this quantity is not a constant property of geophysical systems: different regions of the attractors have different dimensions. Local (also referred to as instantaneous) dimensions can be calculated from the statistics of the neighboring points of a given state. This thanks to a recent breakthrough that has linked Poincaré's recurrence theorem with extreme value theory (Faranda et al., 2017a). In fact, the local dimension is related to the frequency at which a trajectory of the attractor visits an arbitrarily small neighborhood around a given state in the phase space. An advantage of this approach with respect to other commonly used methods (e.g., box counting (Grassberger and Procaccia, 1983)) is that we can investigate locally, i.e., in local regions of the phase space, how many degrees of freedom the system has, and consequently how many variables are needed to characterize the dynamics in each specific region. In other words, in some regions of the attractor the dynamics can be described by only a small number of dofs, while in others a higher number is required. In this way we retrieve information not only on the asymptotic behavior of the attractor (by averaging over time under the ergodic assumption), but also on its local nature.

Global attractor dimensions can be obtained using (i) the Lyapunov dimension (Kaplan and Yorke, 1979) from the Lyapunov spectrum, as well as (ii) the information dimension (Farmer et al., 1983), computed as the average of the local (or pointwise) dimension. These quantities provide the asymptotic (or average) behavior of the attractor. We note that there are several other definitions of attractor dimension, with associated procedures and algorithms to estimate them. Some other methods include the box counting dimension (Grassberger and Procaccia, 1983), and the Hausdorff dimension (Hausdorff, 1919). These were not used in this work.

From the Lyapunov spectrum we can additionally gain information on the possible chaotic nature of the system. Indeed, the Lyapunov exponents characterize the asymptotic behavior of a hypervolume centered around a point on the attractor. If at least one of the dimensions of the hyper-volume stretches asymptotically, then we potentially have sensitivity to initial conditions. This implies limitations on the possibility of making long term predictions because of intrinsic uncertainty in our knowledge of the actual state at previous times (see Table 1 for formal definitions of key terms).

A key challenge when inferring dynamical properties from data, such as the dimensions of the attractor just mentioned, is related to the available observations. These usually consists of time series data of a limited number of variables. In the context of RSF models we may infer or observe the sliding rate and/or the shear stress, but a direct measure of the state variable is challenging. It follows that we do not directly observe the attractor. Nonetheless, from this limited number of variables we can obtain useful properties of the possible generative dynamical system underlying the available data using Taken's embedding theorem (Takens, 1981). Indeed, Taken's embedding theorem allows deriving the attractor dimension even when only a single scalar observable is available, as long as: a) it is linked to the other variables of the system, b) the time series is sufficiently long, and c) it is sampled at a sufficient rate.

Since its formulation, Taken's theorem has been used in a variety of studies involving nonlinear dynamics (Sauer et al., 1991), but a systematic application to earthquake physics is lacking. In the laboratory the limitations stemmed typically from data recording rates, and for earthquake faults from the small number of seismic cycles measured. At natural scale, such limitations have been circumvented studying slow earthquakes, a phenomenon with many similarities with regular earthquakes but with a shorter recurrence time, of the order of weeks or months. The observation of repeated ruptures of the same fault segment enabled the estimation of the system dimension in the Cascadia subduction zone, where slow earthquakes have been found to have on average a reduced number of dofs (< 5) (Gualandi et al., 2020).

Even if stick-slip laboratory experiments have been used extensively to mimic the seismic cycle (Tinti et al., 2016; Leeman et al., 2018), at least two questions are still open: 1) Are slow and regular earthquakes controlled by the same physics? And 2) Is the physics of friction the same at the laboratory and natural scale? Providing a complete answer to these questions is a complicated task that will likely need experiments at multiple spatio-temporal scales, but we can at least verify if slow and fast labquakes live in the same phase space, and if they have a similar number of dof as the one observed for slow earthquakes in nature (< 5) (Gualandi et al., 2020). In this paper, we focus on laboratory experiments, and com-

Table 1
Nonlinear dynamical systems glossary.

Keyword	Description
Dynamical system	A system for which the dynamics can be described via a set of differential equations.
Deterministic system	A dynamical system described by a set of either ordinary differential equations or partial differential equations. Formal definition: A differentiable map Φ or flow $\{\Phi^t\}$ defined on a differentiable manifold $\mathcal{M} \subseteq \mathbb{R}^n$.
Stochastic system	A dynamical system described by a set of stochastic differential equations, i.e. a set of differential equations where at least one term on the right hand side is a stochastic process.
Stochastic process	"A random phenomenon that arises through a process which is developing in time in a manner controlled by probabilistic laws is called a stochastic process. [...] from the point of view of mathematical theory of probability a stochastic process is best defined as a collection $\{X(t), t \in T\}$ of random variables. The set T is called the index set of the process." (Parzen, 2015)
System dimension	Given a dynamical system described by a set of n differential equations, n is the dimension of the system. Formal definition: The dimension of the space into which the differentiable map Φ is defined.
Phase space	Given a dynamical system described by a set of n differential equations, the n variables, that evolve in time according to the associated system, form the so-called phase space. In other words, to fully characterize the state of the system at a given time t, we need n numbers, each corresponding to the value taken by one of the n variables at the specified time t. The n-dimensional space where a point fully characterizes the state of the system is called phase space (or state space).
State vector	Given a dynamical system described by a set of n differential equations, a state vector is an n-dimensional vector belonging to the phase space. The n variables of the state vector are needed to fully characterize the state of the system at a given time t. Note: the state vector does not have to be confused with the state variable (θ) of the rate- and state-friction framework. In fact, θ is one of the variables needed to describe the state of the system. In other words, θ is one of the elements of the state vector, but the state vector is made of other variables as well (e.g., the slip velocity v, the frictional shear stress τ_f, etc.).
Degrees of freedom	Each of the variables belonging to the state vector.
Trajectory	Given a dynamical system described by a set of n differential equations, the evolution in time of the system is described by a sequence of state vectors. The geometrical object described by this sequence is a trajectory.
Attractor	"An invariant set that attracts all the trajectories of the system" (Crauel et al., 1997). In other words, given a trajectory, the set of points towards which the system tends to spend its time. An attractor can be a single point, a line, or a more complicated object (e.g., a so-called strange attractor). By definition, an attractor is a geometrical object that lives in the phase space. It follows that its dimension must be smaller than or equal to the system dimension. Strange attractors have non-integer dimensions.
Poincaré map	Given an attractor, let us take an oriented hyper-plane (i.e., one side will be labeled as negative and the other side as positive) and let us cut the attractor. We call this hyper-plane a Poincaré section. The trajectories will cross the Poincaré section twice: once moving from the negative side to the positive, and once to move in the opposite direction. Let us consider only the points of the attractor that intersect the hyper-plane when passing from the negative side to the positive one. These points will form an ordered set. The Poincaré map is a function that moves one point of the previously defined set to the next. The orange points of Fig. 1 correspond to the above mentioned set obtained via the Poincaré map using the hyper-plane of constant value of τ_f, equal to the average value $\langle \tau_f \rangle$, as Poincaré section.
Lorenz map	Given the time evolution of one of the variables belonging to a dynamical system, the Lorenz map is a function that maps the consecutive local maxima or minima. The cobweb plot is a diagram that helps visualizing the set of points formed by the Lorenz map, and can be seen as the plot of the i-th local maximum/minimum vs the $i+1$-th local maximum/minimum.
Lyapunov spectrum	The Lyapunov spectrum is the set of all Lyapunov exponents.
Lyapunov exponents	Let us consider a point on an attractor. Let us further consider an orthonormal basis centered on the selected point. If we evolve the basis according to the flow, i.e. according to the time evolution imposed by the differential equations governing the system, we obtain a new (potentially deformed) basis. Some directions might be stretched, other contracted. We can then orient the new basis such that the first vector of the basis points towards the direction of maximum stretch. Then we build the second vector of the basis in such a way that the area spanned by the first two basis vectors is stretched the most possible. And so on, we orthonormalize the deformed basis until the n-th vector. Once we have updated the basis, we will evolve it again, but this time following the flow defined in the new point where the trajectory has evolved. Sometimes the basis will stretch in a given direction, and sometimes it will contract. We define the Lyapunov exponents as the tendency to stretch or contract of a given vector of the basis that we have evolved. In other words, the Lyapunov exponents are a concept that represents the long-term asymptotic behavior of expansion/contraction of a hypervolume of the phase space around the attractor.
Lyapunov exponents (formal definition from Benettin et al. (1980))	Let Φ be a differentiable map representing a dynamical system. Given a point on the manifold $\mathcal{M}$, the Lyapunov exponents characterize the asymptotic behavior of the differential $\{d\Phi^t_{\mathbf{x}}\}$. Let $\{E_t\}$ be a family of n-dimensional real vector spaces, with $t \geq 0$. Let us further assume that each vector space has a scalar product $\langle \cdot, \cdot \rangle_t$. If A_t is a linear mapping of E_0 onto E_t $\forall t$, and $\limsup_{t\to\infty} \frac{1}{t} \ln\|A_t\| < \infty$ is always true, with $\|A_t\|$ being the norm of A_t, then we define the Lyapunov characteristic exponent of the vector g with respect to the family $\{A_t\}$ as the quantity $\chi(A_t, g) \stackrel{\text{def}}{=} \limsup_{t\to\infty} \frac{1}{t} \|A_t g\| < \infty$, $\forall g \in E_0$, $g \neq 0$.
Deterministic chaos	Deterministic "chaos is aperiodic behavior in a deterministic system that exhibits sensitive dependence on initial conditions" (Strogatz, 1994). It is commonly stated that a system is governed by deterministic chaos if at least one of its Lyapunov exponents is positive, but a system exhibiting stochastic chaos will also have at least a positive Lyapunov exponent.
Stochastic chaos	Chaotic behavior generated by a stochastic system, i.e. by a set of stochastic differential equations.
Lyapunov time	The inverse of the maximum Lyapunov exponent.
Embedding vector	A vector of dimension m generated by a lower dimensional observed time series. The lower dimensional observation can be a scalar time series or a multivariate time series. In this work we deal with embedding vectors generated by a scalar time series, the friction shear stress τ_f.
Embedding dimension	Dimension m of the embedding vector.

(*continued on next page*)

Table 1 (*continued*)

Keyword	Description
Delay time	When generating the embedding vector, the time delay between points of the observed scalar time series. Here we use standard embedding approaches with constant delay time.
Average dimension	Average of the instantaneous dimension. Because of the ergodic assumption, the time average corresponds to the average in the phase space.
Instantaneous dimension	It is related to how dense is the attractor in a given point of the phase space. To measure it, we consider the neighbors of a given point on the attractor, and estimate the density via extreme value theory and the connection with Poincaré recurrence theorem (Faranda et al., 2017a).

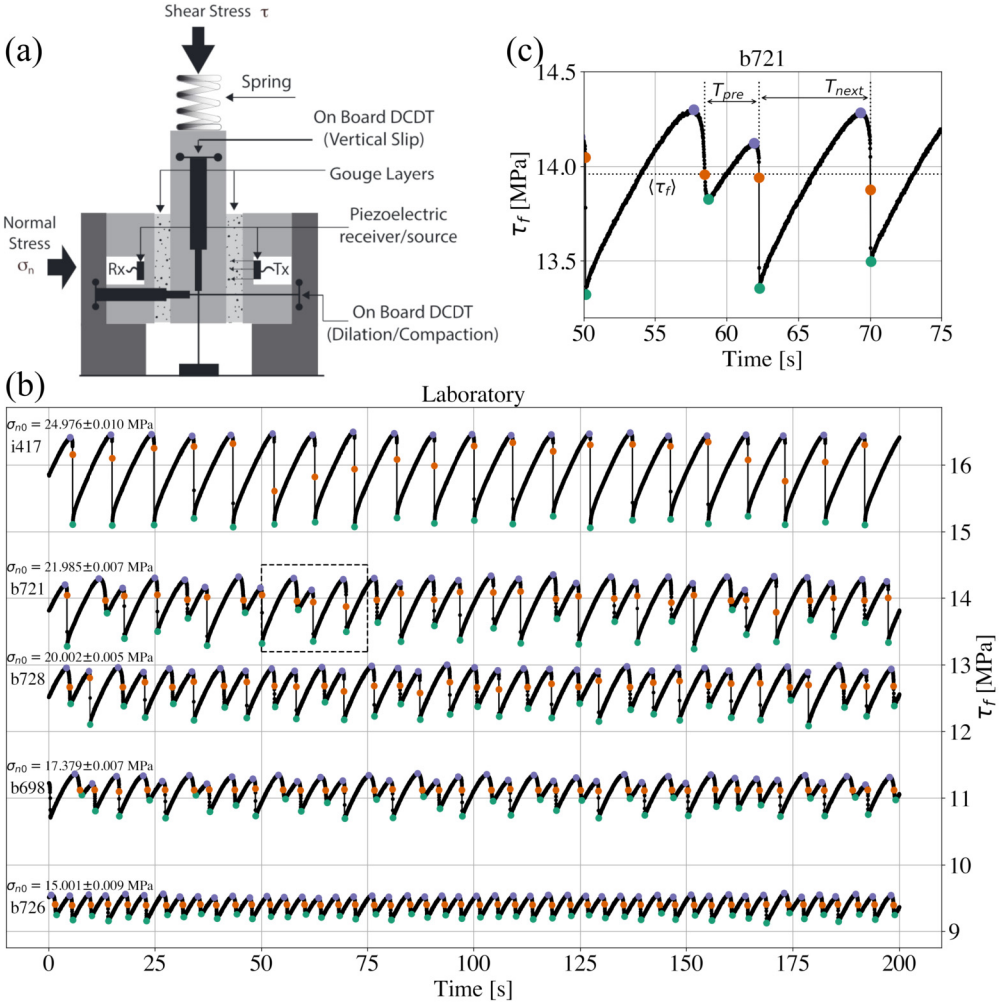

Fig. 1. Experimental set up and data. (a) Sketch of the biaxial apparatus (BRAVA) used for the experiments (Tinti et al., 2016). (b) Frictional shear stress time series (τ_f). Purple/green dots represent local max/min values of τ_f. Orange dots are the closest points during a slip event to the average value of the shear stress $\langle\tau_f\rangle$. (c) Zoom of the black dashed box of panel (b). Interevent (or return) times are taken between the orange dots to reduce sensitivity to measurement noise associated with using max/min values and define the returning of the trajectory to a well specified region of the phase space (i.e., the hyperplane $\tau_f = \langle\tau_f\rangle$).

pare them to slow earthquakes in nature. We find that labquakes and slow natural earthquakes share similar dynamical features. We further find that labquakes can be described by a random attractor (that is: a set of stochastic differential equations). We also argue that our methods can be extended to study frictional dynamical systems at different scales.

The manuscript is organized as it follows. In Section 2 we describe the laboratory data used in the work. In Section 3 we report the obtained results. In particular, in three distinct subsections we comment i) on the estimated dimension, ii) on a plausible low-dimensional model, and iii) on the existence of a random attractor to explain the observations. We conclude the manuscript with discussions and implications of our findings for regular faults. To facilitate connections between earthquake physics and nonlinear system dynamics, we include a glossary of key definitions and concepts (Table 1).

2. Laboratory data

We use data from 14 stick-slip friction experiments conducted at different imposed normal stress (σ_n) conditions (Mele Veedu et al., 2020). In the experiments, two layers of quartz powder are put under σ_n and then sheared using an acrylic piston to modulate the elastic stiffness k around a value (14.8 GPa/m) (Tinti et al., 2016; Mele Veedu et al., 2020) (Fig. 1a). The applied normal stress is used as a control parameter to systematically traverse the critical

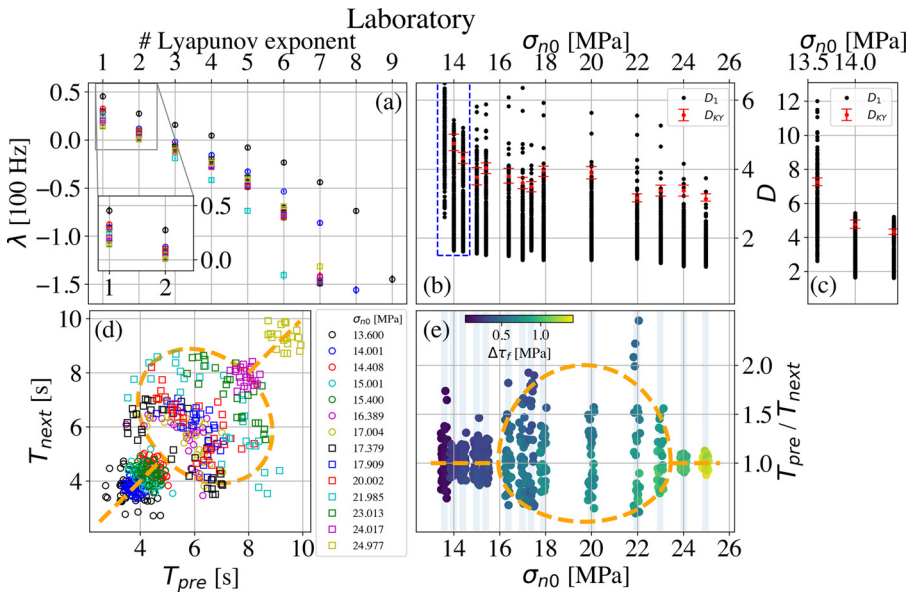

Fig. 2. Results from laboratory data. (a) Lyapunov spectrum estimated from τ_f laboratory data. Legend is shared with panel (d). (b) Lyapunov dimension (D_{KY}) and information dimension (D_1) estimated from τ_f time series. Blue dashed box: results shown in panel (c) with no D saturation for the experiment at lowest σ_{n0}. (d) and (e): bifurcation diagrams using interevent times of the previous and next events. Orange dashed lines indicate hypothetical periodic cycles with one (straight lines) or two (curved lines) events in the cycle. Departure from the dashed lines is evidence of aperiodic behavior.

stability condition for which the stiffness of the loading apparatus (k) is equal to the critical rate of frictional weakening with slip (also called the critical stiffness) of the system ($k_c \propto \frac{1}{\sigma_n}$) (Rice and Ruina, 1983; Gu et al., 1984). In fact, we use data that includes the full transition from stable frictional sliding to slow and fast stick-slip motion. The transition from slow to fast events (Fig. 1b) is defined by the peak sliding velocity during failure, which is dictated by the ratio of $k \gtrsim k_c$ or $k \lesssim k_c$. We provide this information in Tab. S1 in the Supplementary Material.

For normal stresses below 14 MPa slip is stable (e.g., Scuderi et al., 2016). At higher normal stresses, slow stick-slip events (labquakes) occur and these have small stress drop. At intermediate normal stresses, we observe alternating fast and slow events (e.g., Leeman et al., 2016). At the highest normal stress, labquakes are faster with elastodynamic energy release and large amplitude acoustic emissions (Bolton et al., 2020) (Fig. 1b). We use the laboratory observations to determine the number of dofs governing the system with particular focus on changes across the stability transition. We first set up a model with the appropriate number of phase space dimensions to match laboratory data and then explore possible variations for the range of labquake behaviors observed.

Each experiment includes several labquake cycles. We use data in a 200 s time window (Fig. 1 and Tab. S2) in order to have a sufficient number of cycles to perform dynamical systems analysis. We do not extend this window because we do not want to include friction evolution effects associated with shear fabric development and wear. Throughout each experiment, the loading velocity v_0 and the applied σ_n are kept constant to some precision using servo-control. Their mean values and standard deviations are reported in Tab. S2. The nominal v_0 was 10 μm/s for all experiments. Data are sampled every $\Delta t = 0.01$ s.

3. Results

3.1. System dimension

We are interested in retrieving the system dimension (D) because it tells us how many dofs the system has on average. In other words, it carries information on the number of axes that compose the phase space, and consequently indicates how many differential equations we need to characterize the dynamics of the system. To infer D we exploit Takens' embedding theorem (Takens, 1981) and use the scalar time series of the frictional shear stress (τ_f, Fig. 1b-c) since it is the measure with the smallest noise contribution (Tab. S3). We proceed in two different ways. In the first case, we determine the embedding dimension (m) with the method of Cao (1997), and we find values of m ranging from 6 to 9 choosing as an automatic threshold for the metrics E_1 and E_2 a value of 0.9 (Tab. S4). Selecting a higher threshold for the E statistics would provide a higher embedding dimension m (see Fig. S1). We then calculate the Lyapunov dimension (D_{KY}) via the Kaplan-Yorke conjecture (Kaplan and Yorke, 1979), using the Lyapunov spectrum obtained with the method of Sano and Sawada (1985) (Fig. 2a-c). In the second case, we estimate the information dimension (D_1) as the average instantaneous dimension (Faranda et al., 2017b,a) (Fig. 2b-c). Details on the methods are provided in Sec. S1. With both techniques we find in most cases relatively small dimensions (< 5) (Fig. 2b), suggesting that a reduced order model may suffice to explain the observations. The only exception is the experiment at lowest σ_n (Fig. 2c), for which we observe stable creep. In this case the signal to noise ratio (SNR) is low and the retrieved dimension is higher, as expected for noise dominated data. In general, the SNR is increasing the more we increase σ_n, with larger shear stress drops and same level of noise dictated by the recording apparatus. This may explain why we observe an increment in the calculated dimension with smaller normal stresses. Our results are overall consistent with Takens' embedding theorem, for which $m \geq 2D + 1$ (Takens, 1981). Remarkably, a similar low dimension was observed for slow slip events in nature (Gualandi et al., 2020), suggesting that it might be a common feature of frictional faulting across multiple spatio-temporal scales.

3.2. A low-dimensional model

We now seek a low-dimensional model to explain the observations. For a spring-slider model obeying RSF, the number of dofs is 2 plus the number of state variables. Noticing that the dimension of the system tends to decrease with higher σ_n (i.e., for more periodic faster labquakes) (Fig. 2b), we deem reasonable to introduce a radiation damping approximation, where the inertial term

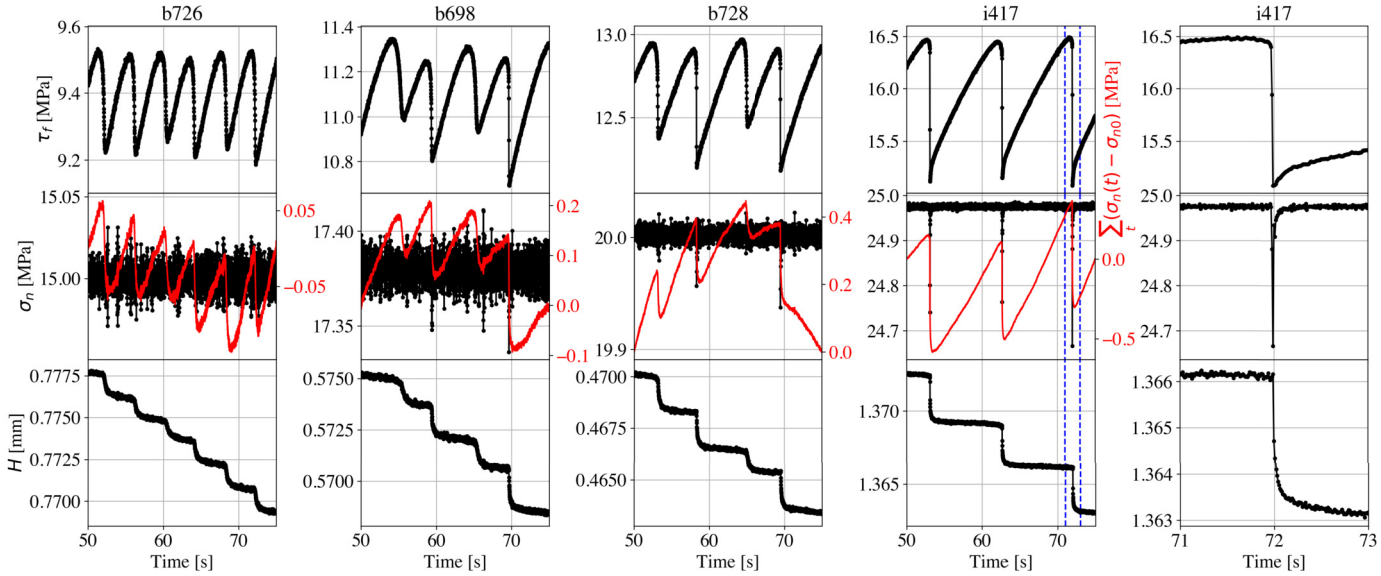

Fig. 3. Shear stress (τ_f, top row), normal stress (σ_n, middle row), and layer thickness (H, bottom row) time evolution for experiments b726 (first column), b698 (second column), b728 (third column) and i417 (fourth column). Red line in second row shows cumulative sum of de-meaned σ_n and reveals perturbations associated with labquakes. Fifth column shows zoom (blue dashed lines in column 4) of experiment i417. Note drop in σ_n of $\sim$0.3 MPa and in H of $\sim$2 μm.

is replaced by a viscous term to represent energy outflow as seismic waves (Rice, 1993) and the number of dofs is reduced by one. Indeed, if inertial effects were important, we would expect fast labquakes to have a higher dimension than slow labquakes. For a non-inertial spring-slider system with RSF and a single state variable it is impossible to get a bifurcation in the slip behavior: the phase space is 2-dimensional, and a closed orbit cannot split into two slipping modes without trajectory intersections occurring in the phase space. An extra variable is needed.

In the classic spring-slider analysis, σ_n is assumed constant, but variations in stress provide one possible explanation for the necessary extra variable. The laboratory data show that σ_n varies slightly for each stress drop (max $\Delta\sigma_n \sim 0.3$ MPa), and this is followed by a short-term recovery of the target σ_{n0} (Fig. 3). During this time the fault zone thickness (H) also varies, showing both immediate and slip (time) dependent compaction after a stress drop (Fig. 3). The variations in H are a function of relaxation of shear-induced dilation (Marone et al., 1990), layer thinning (Scott et al., 1994), and the drop in σ_n that occurs as the servo-control system responds to the labquake. We did not study partitioning between these causes but rather accounted for them using the formalism of Segall and Rice (1995) for porous materials, where porosity (ϕ) and pore pressure (p) are introduced as variables in the dynamics and linked to σ_n via Terzaghi's principle (Terzaghi, 1925). We introduce the possibility for the characteristic distance over which the porosity relaxes (L_ϕ) to differ from the RSF characteristic slip distance (L). The model is summarized by the following set of non-dimensional ordinary differential equations (ODE) (see section S2.1 for its derivation):

$$\dot{x} = \frac{e^x\left[(\beta_1 - 1)\,x\,(1+\lambda u) + y - u\right] + \kappa\left(\frac{v_0}{v_*} - e^x\right) - \dot{u}\,\frac{1+\lambda y}{1+\lambda u}}{1 + \lambda u + \nu e^x} \tag{1a}$$

$$\dot{y} = \kappa\left(\frac{v_0}{v_*} - e^x\right) - \nu e^x \dot{x} \tag{1b}$$

$$\dot{z} = -\rho e^x(\beta_2 x + z) \tag{1c}$$

$$\dot{u} = -\alpha - \gamma u + \dot{z} \tag{1d}$$

The state vector $\boldsymbol{\zeta}$, i.e. that vector that fully characterizes the state of the system, is made of the non-dimensional variables $[x, y, z, u] = \left[\ln\left(\frac{v}{v_*}\right), \frac{\tau_f - \tau_0}{a\sigma_{n0}}, \frac{1}{\lambda\beta\sigma_{n0}}(\phi - \phi_0), -\frac{1}{\lambda}\frac{p}{\sigma_{n0}}\right]$, where v_* is a reference sliding velocity, $\tau_0 = \mu_0\sigma_{n0}$ is the product of the reference friction coefficient μ_0 and the reference normal stress σ_{n0}, λ is equal to $\frac{a}{\mu_0}$ with a being the RSF direct effect parameter (i.e., the instantaneous response of the friction coefficient to a sudden step in the sliding velocity), β is the product of the elastic component of porosity and the combined compressibility of the fluid in the pores and the elastic pores, and ϕ_0 is a reference porosity. The other parameters appearing in system (1) are the ratio between the RSF evolutionary and direct effect parameters $\beta_1 = \frac{b}{a}$, the non-dimensional spring stiffness κ, viscous parameter ν, dilatancy coefficient β_2, pore pressure in the surrounding α, diffusivity γ, and the ratio $\rho = \frac{L}{L_\phi}$.

The parameters selection is described in Section S3.1, and is largely based on values taken from the literature (Figs. S2-S5). For the preferred parameters and the tested σ_{n0}, the solution of the ODE system does not show chaotic behavior. Instead, labquakes occur periodically with either a single characteristic time or as a characteristic sequence of slow and fast events (Figs. 4a, d, e). In other words, with the adopted parameters the system exhibits a cyclic attractor and a limit cycle (Fig. 5d). We notice that a quasi-static spring-slider system with two RSF state variables is a particular case of the set of ODE previously derived, with the second state variable being either the porosity or the pore pressure (see section S2.2). Such a system shows the typical behavior of the route to chaos within a narrow range of the stability control parameter, culminating in instability and divergence of the solution when sufficiently reducing the stiffness of the system κ (i.e., when increasing σ_{n0}) (Becker, 2000). The modified approach with quasi-dynamic approximation, two state variables, and two characteristic relaxation distances allows us to avoid numerical divergence and reproduce the major features of the laboratory data, including period doubling followed by a return to a single characteristic labquake cycle as σ_{n0} increases (Figs. 4d-e). To obtain these results we used a radiation damping term 20 times larger than the commonly adopted value, which assumes an infinite fault plane in an elastic full space and radiation due only to outgoing planar shear waves (Rice, 1993). The experiments we use were conducted

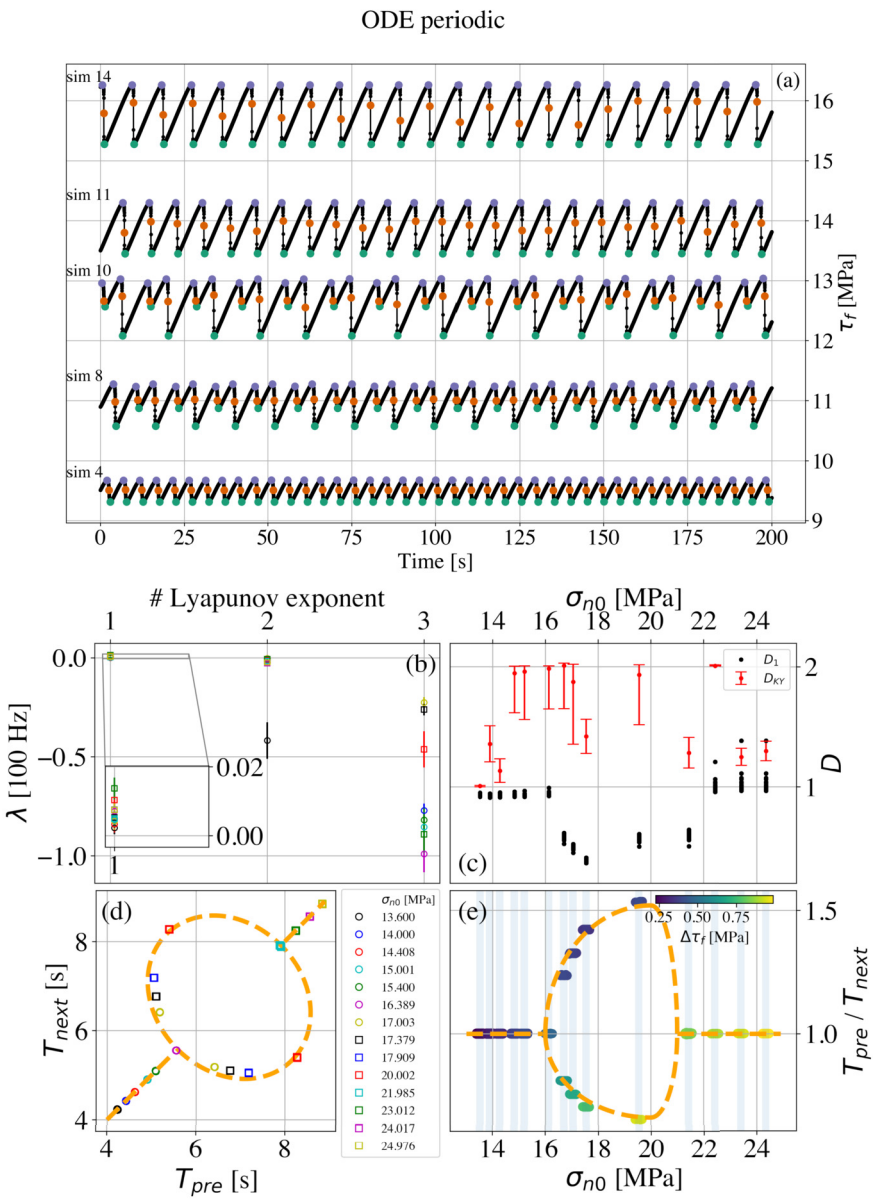

Fig. 4. As Figs. 1b and 2, but for ODE simulated time series via the system of eqs. 1. Simulations 4, 8, 10, 11, and 14 use imposed σ_{n0} to mimic experiments b726, b698, b728, b721 and i417. The system is periodic with either a single or double period, as highlighted by the orange dotted lines in panels (d) and (e). A slightly positive maximum Lyapunov exponent may be due to the temporal sampling used to mimic laboratory observations (0.01 s): to fully resolve the dynamical evolution we need smaller time steps, and a calculated positive Lyapunov exponent is not sufficient to claim the presence of chaotic behavior.

on porous gouge with a finite thickness that evolves over time. This suggests that in the laboratory with simulated fault zones that are a few mm in thickness, a larger fraction of energy might be dissipated in so-called spectator regions of the fault zone that are adjacent to localized zones of shear (Collettini et al., 2009). Changing the parameters can lead to deterministic chaos, but typically only for a narrow range of σ_{n0} (see simulation 8 in Fig. 6a, corresponding to $\sigma_{n0} = 17.379$ MPa in Figs. 6d-e). We do not exclude the possibility that part of the observed irregularity may be due to this transition to deterministic chaos. This irregularity can be seen from Fig. 2 where we plot for each event the time to the next event (T_{next}) vs the time since the previous event (T_{pre}) (panel d) and the ratio $\frac{T_{pre}}{T_{next}}$ as a function of σ_{n0} (panel e). Fig. 2d in particular is an example of a cobweb plot, in the specific for the interevent time. In Fig. S6 we show the same plot but for each experiment in a separate subplot, to better appreciate the details. Another interesting measure is the stress drop, for which a cobweb plot is shown in Fig. S7. In the aforementioned plots we see a spread of points around the values that would represent periodic cycles of loading and failure (orange dashed lines in Figs. 2d-e). Aperiodicity can also be measured via the Coefficient of Variation (CV), defined as the ratio between the standard deviation and the mean of the observed interevent times (Fig. 5a). Measuring the CV using the recurrence time of subsequent ruptures it is possible to obtain high CVs also for periodic sequences of slow-fast events, as is also the case for ODE simulations in the period doubling parameter region.

Period doubling as well as fast and slow events can be obtained with models either containing many more dofs with respect to the spring-slider (Mele Veedu et al., 2020; Cattania, 2019; Luo and Ampuero, 2018), and many more than those deducible from the observed time series, or with geometrical complexities (Romanet et al., 2018). Our model has the following relevant characteristics: (1) reproduces the appropriate range of shear stress drops, (2) reproduces the bifurcation at the same σ_{n0} values actually imposed

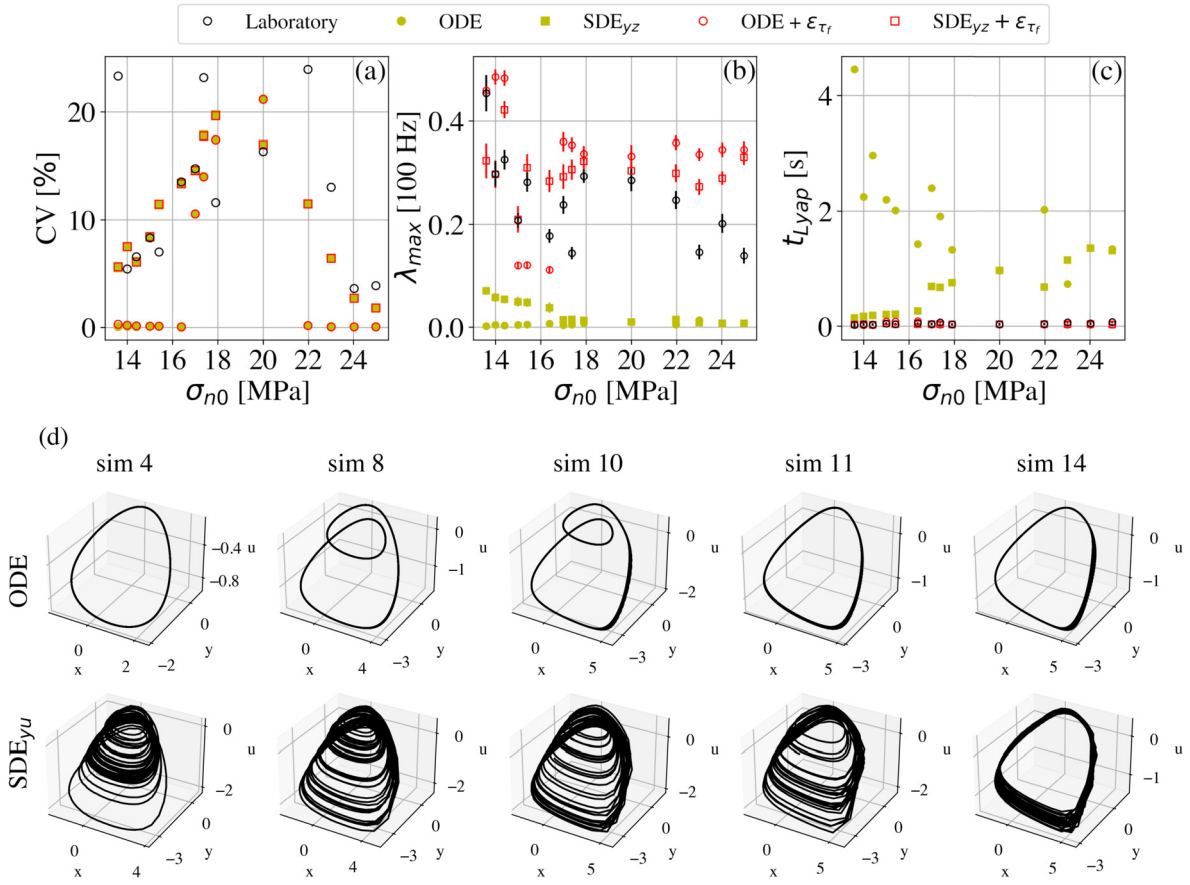

Fig. 5. (a) CV (in %), (b) maximum Lyapunov exponent (λ_{max}) and (c) Lyapunov time ($t_{Lyap} = \frac{1}{\lambda_{max}}$) for the laboratory and simulated friction shear stress time series. (d) Phase space subregion xyu of the ODE (top) and SDE (bottom) simulations with imposed σ_{n0} to mimic experiments b726, b698, b728, b721 and i417.

in the laboratory, (3) uses a number of dofs in agreement with the one derived from the observations, and (4) takes into account variations in σ_{n0} (even if not perfectly, see Figs. S2-S5b to see how τ_f and σ_n vary when changing the parameters). We thus use the low-dimensional model to describe the observations rather than a more sophisticated model representative of a high-dimensional extension to the continuum.

3.3. Random attractor

Laboratory data are more irregular than the ODE simulations: the events far from the transition regime show a single characteristic cycle, but with a return time not always exactly the same (Figs. 2d-e and 5a). We notice that σ_n and τ_f are subject to high-frequency noise fluctuations (Figs. 3 and 7). An analysis of the residual time series relative to the experiment exhibiting creep ($\sigma_{n0} = 13.6$ MPa) reveals a Gaussian noise with $\varepsilon_{\sigma_{n0}} = \text{std}(\sigma_n - \sigma_{n0}) = 0.006$ MPa and $\varepsilon_{\tau_f} = \text{std}(\tau_f - \tilde{\tau}_f) = 0.004$ MPa, where $\tilde{\tau}_f$ is a cubic spline approximation used to smooth the time series and filter out the low frequencies (Fig. 7). These fluctuations can be due to observational noise, but can also perturb the stress field affecting the system dynamics. In fact, adding only observational noise to the ODE simulations explains neither the observed irregularities (compare Figs. 2d-e, S6, S7, and S8d-e) nor the CV variability since the ODE with a single characteristic labquake show a null CV (Fig. 5a). Given the Gaussian nature of the residual time series, we modify the ODE related to τ_f and σ_n (i.e., y and u) substituting the equations with a pair of Stochastic Differential Equations (SDE), with the stochastic term described by a Wiener process W_T (a real-valued continuous-time stochastic process) of intensity ε_y and ε_u:

$$\mathrm{d}y = \left[\kappa\left(\frac{v_0}{v_*} - e^x\right) - \nu e^x \dot{x}\right]\mathrm{d}T + \varepsilon_y \mathrm{d}W_T \tag{2a}$$

$$\mathrm{d}u = [-\alpha - \gamma u + \dot{z}]\,\mathrm{d}T + \varepsilon_u \mathrm{d}W_T \tag{2b}$$

ε_y and ε_u can be modulated to introduce more or less noise to the dynamics. We set them to half of the non-dimensionalized data-derived standard deviation because ε_{σ_n} and ε_{τ_f} can be considered as an upper bound for the intensity of the perturbations to the dynamics. The simulated time series are shown in Fig. S9. Also v and ϕ (i.e., x and z) may be subject to noise that can perturb the dynamics of the system. Contrary to τ_f and σ_n, we do not directly measure them. Before introducing further complications, we consider the noises on σ_n and τ_f as the most relevant ones. To mimic the laboratory time series, we finally add measurement noise of ε_{τ_f} to the SDE generated τ_f time series (Fig. 8a). The Lyapunov spectrum, the system dimension, and the interevent times are shown in Figs. 8b-e. We find a Lyapunov spectrum similar to the one derived from the data, D_{KY} typically between 3 and 4, and both D_{KY} and D_1 decreasing with increasing σ_{n0} (see Fig. 2b for comparison). Furthermore, in the bifurcation diagrams we see a spread similar to the one observed in the laboratory time series. This result suggests that the aperiodicities in the returning time of laboratory earthquakes (of any type, either slow or fast or mixed) could be the result of a stochastic noise component that enters the dynamics and gets amplified due to the nonlinearities of the equations. As a consequence, with the current available laboratory set up, stick-slip cycles near the critical transition regime

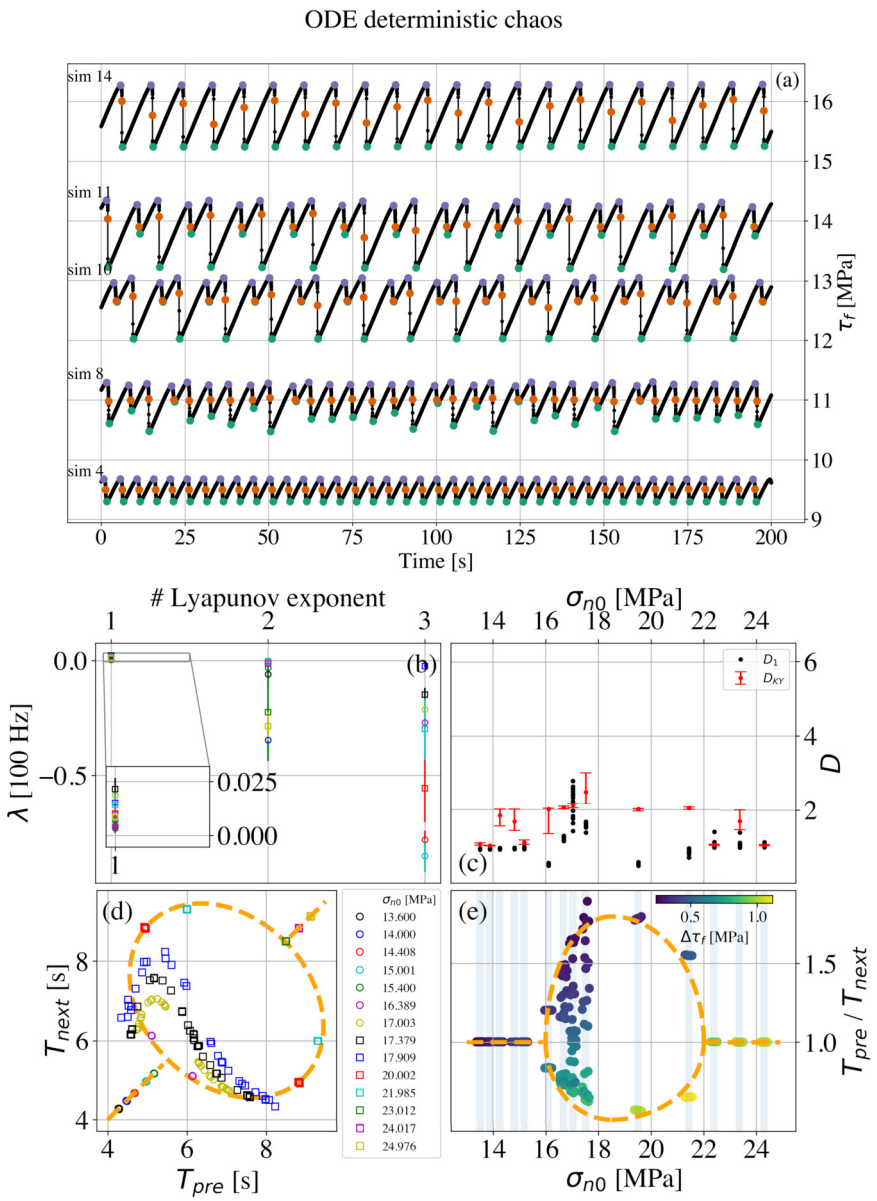

Fig. 6. As Fig. 4 but using $\nu = 15\nu_0$ instead of $\nu = 20\nu_0$. Notice that with this parameter the system shows deterministic chaos, highlighted by the departure from the orange dotted lines (panels d and e), even if only in a narrow range of σ_{n0}.

are reproducible only statistically and not deterministically, in the sense that, with the same rocks and conditions applied, we can expect to reproduce similar average interevent times and standard deviations, but not the same exact sequence of ruptures. Similar observations were made for a different frictional system of labquakes (Karner and Marone, 2000), and this type of feedback between the apparatus' vibrations and the system dynamics has been documented for turbulent flows (Faranda et al., 2017b). These behaviors may be a more general characteristic of nonlinear frictional systems.

We further notice that the addition of a stochastic term to the dynamics induces a bifurcation for a wider range of σ_{n0}, leading periodic single-rupture scenarios to slip with a mixture of slow and fast modes (see the experiments at $20 < \sigma_{n0} < 23$ MPa, Fig. 4 or S8 for ODE simulations and Fig. 8 or S9 for SDE).

4. Implications and future perspectives

Our results suggest the existence of a random attractor (Fig. 5d) to describe the seismic cycle. Minimal variations of the order 0.05% of the shear and normal stresses applied to the fault (intended as the experimental frictional interface) influence the large scale dynamics and the recurrence time of labquakes, inducing CV of a few percent points ($\gtrsim 2\%$, Fig. 5a). The implications for natural faults are significant. At seismogenic depths (~ 10 km), variations of $\lesssim 0.05\%$ of the lithostatic stress would correspond to $\lesssim 150$ kPa. Possible causes that can generate stress perturbations of 10-100 kPa (or more) are: other tectonic sources (with both static and dynamic stress variations (Freed, 2005)), magmatic intrusions in volcano-tectonic environments (Chen et al., 2019), surface atmospheric loading (D'Agostino et al., 2018; Pintori et al., 2021), anthropogenic activity, and tides (Rubinstein et al., 2008). The laboratory experiments here considered were conducted to explore the transition between linearly stable to unstable behavior ($\frac{k}{k_c} \sim 1$), likely similar to the one where episodic tremors are observed in nature since the studied labquakes have similar dimensions to slow earthquakes in Cascadia (Gualandi et al., 2020). Given that k_c depends on σ_n (Rice and Ruina, 1983), variations ε_{σ_n} influence the stability of the system as seen by the induced slow-fast ruptures

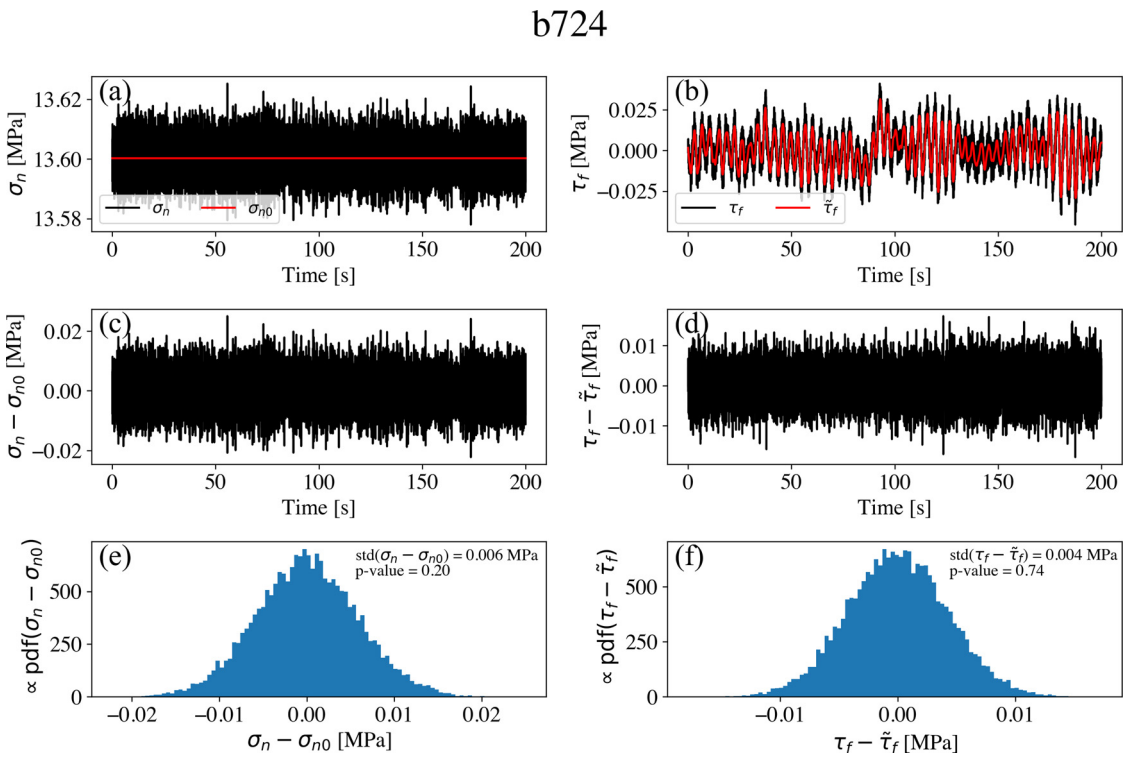

Fig. 7. Noise analysis for σ_n (left) and τ_f (right) for experiment b724. a) and b): Original data (black) and subtracted value (red, equal to the average normal stress σ_{n0} on the left and a cubic spline smoothing of the shear stress $\tilde{\tau}_f$ on the right). c) and d): Residual time series representative of the high frequency noise. e) and f): Histograms of the residual time series c) and d). The standard deviation and the p-value derived from a Shapiro-Wilk test are also reported. The analysis suggests that, at a standard significance level of 0.05, we cannot reject the null hypothesis for which the residual distribution of both the normal stress and the friction shear stress were drawn from a normal distribution. For this reason we use as representative of the noise the standard deviations derived from this analysis.

in otherwise single-cycle experiments, suggesting that we should not treat faults as isolated systems, especially when modeling the limits of the seismogenic zone in nature.

The lack of an appropriate deterministic description of all the aforementioned stress perturbations may explain why earthquake forecast is a difficult task and statistical methods are used (Main, 1996, 1999). The addition of the available physical information is a fundamental aspect to improve our forecasts. Our results relying on laboratory experiments may explain why a mix of physical knowledge and statistical methods like those obtained with a Brownian Relaxation Oscillator (BRO) (Matthews et al., 2002) are often used for earthquakes forecast (Ogata, 2017). Compared to the BRO, we have introduced the stochastic perturbations under a more rigorous physical description of friction, i.e. under the RSF framework using two length-scale parameters. Despite a low average dimension of the attractor (typically < 5, Fig. 2b), the maximum instantaneous dimension deduced from the data ranges from ~ 12 (experiment b727, $\sigma_{n0} = 24.017$ MPa) to ~ 47 (experiment b695, $\sigma_{n0} = 17.909$ MPa). This suggests that extra dofs are needed to fully characterize the dynamics in some regions of the phase space. Supplying a stochastic term to the dynamics is an admittance of our ignorance on how to monitor and describe these extra dofs (Vere-Jones et al., 2005). The maximum instantaneous dimension increases from ~ 2 to ~ 41 when perturbing the ODE dynamics with a stochastic term, and it reaches ~ 82 when introducing also observational noise. The choice of modeling small scale fluctuations via stochastic terms is not unique, and deterministic descriptions could hold as well. Whether solids and fluids should be phenomenologically modeled via stochastic or deterministic equations is still an open problem (Nath et al., 2009; Cruzeiro, 2020) which affects, for example, the quality of weather forecasts and climate predictions (Palmer, 2019). Another limitation may come from the fact that instabilities are introduced by inertial effects, here neglected but needed to describe natural earthquakes. Despite these limitations, the proposed description explains major features of the laboratory shear stress time series and reconciles the number of dofs that can be deduced from the observations. Furthermore, this model explains fluctuations of the labquakes stress drop caused by the inclusion of stochastic perturbations to the dynamics, thus contributing to the debate on stress drop scaling with earthquake size (Cocco et al., 2016). Thanks to the ODE and SDE models, we can estimate the effect of the stochastic term to the predictability of the dynamics. The Lyapunov time (t_{Lyap}) is limited for ODE models (~ 2 s on average) due to the finite Δt, and it is reduced for SDE models (~ 0.6 s on average). We notice a peculiar trend of t_{Lyap} with σ_{n0}. In particular, t_{Lyap} gets smaller when increasing σ_{n0} for ODE simulations, while it gets larger for SDE simulations (Fig. 5c). This means that for ODE the predictability horizon is larger for slow events and smaller for fast events. This can be understood in terms of the instability duration. Slow events are seen as more predictable because the differential of the system varies less abruptly than that for fast events. This means that even when we are not able to properly estimate the tangent map because of coarse temporal sampling, if the dynamics are slow then the error is smaller than for the fast dynamics with the same temporal sampling. On the other hand, for SDE simulations we observe the opposite trend for t_{Lyap}. This can be explained by the fact that the shear and normal stresses for fast events are larger than those for slow events, but the stochastic fluctuations introduced to perturb the dynamics have the same amplitude independently of the applied normal stress. It follows that these perturbations are more relevant for slow events, making them more stochastic and thus less predictable. This observation has relevant implications for frictional sliding at natural scale. In fact, we can imagine that small scale fluctuations of the stress field play a more relevant role for slow earthquakes than for

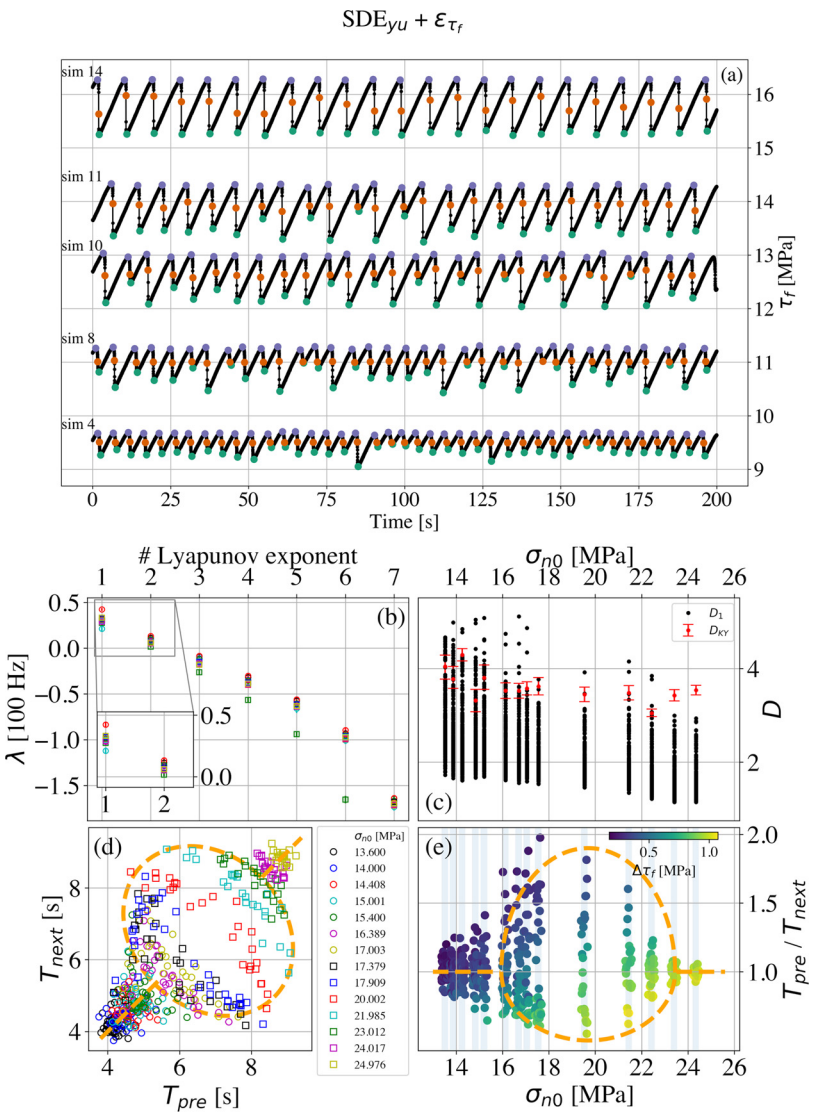

Fig. 8. (a) Frictional shear stress τ_f simulated using the system of SDE with stochastic terms added to y and u, and addition of observational noise ε_{τ_f} on τ_f. Simulations 4, 8, 10, 11, and 14 use imposed σ_{n0} to mimic experiments b726, b698, b728, b721 and i417. (b)-(e): As Fig. 2, but for SDE simulated time series with stochastic terms added to y and u and the addition of observational noise ε_{τ_f} on τ_f. The aperiodic behavior highlighted by the departure from the orange dotted lines is now a common feature at all values of σ_{n0}, similar to the laboratory observations.

fast, elastodynamic earthquakes. This does not exclude though that the irregularity introduced in the recurrence of slow earthquakes can then be transmitted to larger scale, influencing regular earthquakes recurrence, especially close to the brittle-ductile transition zone where slow slip events can trigger regular earthquakes (e.g., Radiguet et al., 2016).

Data-driven model-free techniques have been used to predict the behavior of chaotic systems. Examples are offered by the Nonlinear Forecasting Analysis (Farmer and Sidorowich, 1987; Casdagli, 1989; Wales, 1991), reservoir computing approaches (Pathak et al., 2018), Long-Short Term Memory (LSTM) recurrence neural networks and transformer networks (Laurenti et al., 2022). While these approaches provide a forecasted value, sometimes in good agreement with the observations even up to $8t_{Lyap}$ into the future (Pathak et al., 2018), they are often used as black boxes, and the interpretability of the analysis is unclear. To have a better understanding of the physics behind a prediction, as future steps we envision the application of data assimilation (DA) approaches that can use the model here presented to advance the state of the system. The major challenge for a DA approach comes from the lack of measure of the variables needed to fully describe the state of the system. Recent advances linking embedding theory to the Frenet-Serret description of a dynamical system have been proposed based on the Hankel view of Koopman (HAVOK) theory (Brunton et al., 2017; Hirsh et al., 2021). This approach takes advantage of Taken's embedding theory (Takens, 1981; Sauer et al., 1991) and converts an autonomous nonlinear system into a non-autonomous linear system with an additional nonlinear forcing term. Given the overall low dimension retrieved for the system under study, a plausible next step will be to investigate reduced order models like the aforementioned one. Similar to weather forecast, we think that ensemble forecast is the most reasonable way to assess the future state of the system because of the unavoidable stochastic terms that affect the dynamics. Early attempts of earthquake ensemble forecast can be found in Marzocchi et al. (2012) and references therein. Differently from previous models, which were purely based on statistical seismology, we simulate aperiodic behavior incorporating the physics of friction via the RSF formalism. We do not exclude using this model to improve laboratory earthquakes forecast with machine learning approaches, generat-

ing at will synthetic data that resembles the major characteristics of the observed time series and reducing the shortcoming of limited training datasets.

CRediT authorship contribution statement

A. Gualandi: Conceptualization, Formal analysis, Methodology, Software, Validation, Visualization, Writing – original draft. **D. Faranda:** Conceptualization, Validation, Writing – review & editing. **C. Marone:** Funding acquisition, Writing – review & editing. **M. Cocco:** Writing – review & editing. **G. Mengaldo:** Conceptualization, Validation, Writing – review & editing.

Declaration of competing interest

The authors declare that they have no known competing financial interests or personal relationships that could have appeared to influence the work reported in this paper.

Data availability

Data are publicly available from previous publication. The code to reproduce the results is available at https://github.com/Geolandi/labquakesde.

Acknowledgements

We thank Carolina Giorgetti, Luca Dal Zilio, Giacomo Pozzi, Lauro Chiaraluce and Marco Maria Scuderi for insightful discussions. We thank the Editor Rebecca Bendick and two anonymous reviewers for their valuable comments. AG and CM were supported by European Research Council Advance Grant 835012 (TECTONIC). MC participated in this work as Principal Investigator of the European Research Council (ERC) project FEAR (grant 856559) under the European Community's Horizon 2020 Framework Programme. GM acknowledges support from NUS Startup Grant 22-3565-A0001-1, and MOE Tier 2 Grant 22-5191-A0001-0.

Appendix A. Supplementary material

Supplementary material related to this article can be found online at https://doi.org/10.1016/j.epsl.2023.117995.

References

Barbot, S., 2022. A rate-, state-, and temperature-dependent friction law with competing healing mechanisms. J. Geophys. Res., Solid Earth, e2022JB025106.
Baumberger, T., Caroli, C., 2006. Solid friction from stick–slip down to pinning and aging. Adv. Phys. 55 (3–4), 279–348. https://doi.org/10.1080/00018730600732186.
Becker, T., 2000. Deterministic chaos in two state-variable friction sliders and the effects of elastic interactions. In: Geocomplexity and the Physics of Earthquakes. In: Geophysical Monograph, vol. 120. AGU.
Benettin, G., Galgani, L., Giorgilli, A., Strelcyn, J.-M., 1980. Lyapunov characteristic exponents for smooth dynamical systems and for Hamiltonian systems; a method for computing all of them. Part 1: theory. Meccanica 15 (9).
Bizzarri, A., Cocco, M., 2006. A thermal pressurization model for the spontaneous dynamic rupture propagation on a three-dimensional fault: 1. Methodological approach. J. Geophys. Res. 111, B05303. https://doi.org/10.1029/2005JB003862.
Bolton, D.C., Shreedharan, S., Riviére, J., Marone, C., 2020. Acoustic energy release during the laboratory seismic cycle: insights on laboratory earthquake precursors and prediction. J. Geophys. Res., Solid Earth 125, e2019JB018975. https://doi.org/10.1029/2019JB018975.
Brunton, S., Brunton, B., Proctor, J., Kaiser, E., Kutz, J., 2017. Chaos as an intermittently forced linear system. Nat. Commun. 8 (1). https://doi.org/10.1038/s41467-017-00030-8.
Burridge, R., Knopoff, L., 1967. Model and theoretical seismicity. Bull. Seismol. Soc. Am. 57, 341–371.
Cao, L., 1997. Practical method for determining the minimum embedding dimension of a scalar time series. Physica D 110, 43–50.
Casdagli, M., 1989. Nonlinear prediction of chaotic time series. Physica D 35, 335–356.
Cattania, C., 2019. Complex earthquake sequences on simple faults. Geophys. Res. Lett. 46, 10384–10393. https://doi.org/10.1029/2019GL083628.
Chen, K., Smith, J., Avouac, J., Liu, Z., Song, Y., Gualandi, A., 2019. Triggering of the mw 7.2 Hawaii earthquake of 4 may 2018 by a dike intrusion. Geophys. Res. Lett. 46, 2503–2510. https://doi.org/10.1029/2018GL081428.
Cocco, M., Tinti, E., Cirella, A., 2016. On the scale dependence of earthquake stress drop. J. Seismol. 20 (3). https://doi.org/10.1007/s10950-016-9594-4.
Collettini, C., Niemeijer, A., Viti, C., Marone, C., 2009. Fault zone fabric and fault weakness. Nature 462, 907–910. https://doi.org/10.1038/nature08585.
Crauel, H., Debussche, A., Flandoli, F., 1997. Random attractors. J. Dyn. Differ. Equ. 9 (2).
Cruzeiro, A., 2020. Stochastic approaches to deterministic fluid dynamics: a selective review. Water 12 (3), 864.
D'Agostino, N., Silverii, F., Amoroso, O., Convertito, V., Fiorillo, F., Ventafridda, G., Zollo, A., 2018. Crustal deformation and seismicity modulated by groundwater recharge of karst aquifers. J. Geophys. Res., Solid Earth 45 (22), 12253–12262. https://doi.org/10.1029/2018GL079794.
Dal Zilio, L., Lapusta, N., Avouac, J.-P., 2020. Unraveling scaling properties of slow-slip events. Geophys. Res. Lett. 47, e2020GL087477. https://doi.org/10.1029/2020GL087477.
Dieterich, J., 1979. Modeling of rock friction, 1, experimental results and constitutive equations. J. Geophys. Res. 8, 2161–2168.
Faranda, D., Messori, G., Yiou, P., 2017a. Dynamical proxies of North Atlantic predictability and extremes. Sci. Rep. 7, 41278. https://doi.org/10.1038/srep41278.
Faranda, D., Sato, Y., Saint-Michel, B., Wiertel, C., Padilla, V., Dubrulle, B., Daviaud, F., 2017b. Stochastic chaos in a turbulent swirling flow. Phys. Rev. Lett. 119, 014502. https://doi.org/10.1103/PhysRevLett.119.014502.
Farmer, J., Sidorowich, J., 1987. Predicting chaotic time series. Phys. Rev. Lett. 59 (8).
Farmer, J., Ott, E., Yorke, J., 1983. The dimension of chaotic attractors. Phys. D: Nonlinear Phenom. 7 (1–3), 153–180. https://doi.org/10.1016/0167-2789(83)90125-2.
Freed, A., 2005. Earthquake triggering by static, dynamic, and postseismic stress transfer. Annu. Rev. Earth Planet. Sci. 33 (1), 335–367. https://doi.org/10.1146/annurev.earth.33.092203.122505.
Grassberger, P., Procaccia, I., 1983. Characterization of strange attractors. Phys. Rev. Lett. 50 (5). https://doi.org/10.1103/PhysRevLett.50.346.
Gu, J.-C., Rice, J., Ruina, A., Tse, S., 1984. Slip motion and stability of a single degree of freedom elastic system with rate and state dependent friction. J. Mech. Phys. Solids 32 (3), 167–196.
Gualandi, A., Avouac, J.-P., Michel, S., Faranda, D., 2020. The predictable chaos of slow earthquakes. Sci. Adv. 6 (27). https://doi.org/10.1126/sciadv.aaz5548.
Hausdorff, F., 1919. Dimension und äußeres maß. Math. Ann. 79 (2), 157–179.
Hirsh, S., Ichinaga, S., Brunton, S., Kutz, N., Brunton, B., 2021. Structured time-delay models for dynamical systems with connections to Frenet–Serret frame. Proc. R. Soc. A 477, 20210097. https://doi.org/10.1098/rspa.2021.0097.
Huang, J., Turcotte, D.L., 1990. Evidence for chaotic fault inter- actions in the seismicity of the San Andreas fault and Nankai trough. Nature 348, 234–236.
Im, K., Saffer, D., Marone, C., Avouac, J.-P., 2020. Slip-rate-dependent friction as a universal mechanism for slow slip events. Nat. Geosci. 13, 705–710. https://doi.org/10.1038/s41561-020-0627-9.
Kaplan, J., Yorke, J., 1979. Chaotic behavior of multidimensional difference equations. In: Peitgen, H.O., Walther, H.O. (Eds.), Functional Differential Equations and the Approximation of Fixed Points. In: Lecture Notes in Mathematics. Springer, pp. 204–227.
Karner, S., Marone, C., 2000. Effects of loading rate and normal stress on stress drop and stick-slip recurrence interval. In: Geocomplexity and the Physics of Earthquakes. In: Geophysical Monograph, vol. 120. AGU.
Lapusta, N., Liu, Y., 2009. Three-dimensional boundary integral modeling of spontaneous earthquake sequences and aseismic slip. J. Geophys. Res. 114, B09303. https://doi.org/10.1029/2008JB005934.
Laurenti, L., Tinti, E., Galasso, F., Franco, L., Marone, C., 2022. Deep learning for laboratory earthquake prediction and autoregressive forecasting of fault zone stress. Earth Planet. Sci. Lett. 598. https://doi.org/10.1016/j.epsl.2022.117825.
Leeman, D., Saffer, J.R., Scuderi, M., Marone, C., 2016. Laboratory observations of slow earthquakes and the spectrum of tectonic fault slip modes. Nat. Commun. 7, 11104. https://doi.org/10.1038/ncomms11104.
Leeman, J., Marone, C., Saffer, D., 2018. Frictional mechanics of slow earthquakes. J. Geophys. Res. 123 (9). https://doi.org/10.1029/2018JB015768.
Li, Q., Tullis, T., Goldsby, D., Carpick, R., 2011. Frictional ageing from interfacial bonding and the origins of rate and state friction. Nature 480, 233–236. https://doi.org/10.1038/nature10589.
Linker, M., Dieterich, J., 1992. Effects of variable normal stress on rock friction: observations and constitutive equations. J. Geophys. Res. 97 (B4), 4923–4940.
Luo, Y., Ampuero, J.-P., 2018. Stability of faults with heterogeneous friction properties and effective normal stress. Tectonophysics 733, 257–272. https://doi.org/10.1016/j.tecto.2017.11.006.
Main, I., 1996. Statistical physics, seismogenesis, and seismic hazard. Rev. Geophys. 34 (4), 433–462. https://doi.org/10.1029/96RG02808.

Main, I., 1999. Earthquake prediction: concluding remarks. Nature. https://doi.org/10.1038/nature28133.
Mair, K., Marone, C., 1999. Friction of simulated fault gouge for a wide range of velocities and normal stresses. J. Geophys. Res., Solid Earth 104, 28899–28914.
Marone, C., Kilgore, B., 1993. Scaling of the critical slip distance for seismic faulting with shear strain in fault zones. Nature 362, 618–621.
Marone, C., Raleigh, C., Scholz, C., 1990. Frictional behavior and constitutive modeling of simulated fault gouge. J. Geophys. Res., Solid Earth 95 (B5), 7007–7025. https://doi.org/10.1029/JB095iB05p07007.
Marzocchi, W., Zechar, D., Jordan, T., 2012. Bayesian forecast evaluation and ensemble earthquake forecasting. Bull. Seismol. Soc. Am. 102 (6), 2574–2584. https://doi.org/10.1785/0120110327.
Matthews, M., Ellsworth, W., Reasenberg, P., 2002. A Brownian model for recurrent earthquakes. Bull. Seismol. Soc. Am. 92 (6), 2233–2250.
Mele Veedu, D., Giorgetti, C., Scuderi, M., Barbot, S., Marone, C., Collettini, C., 2020. Bifurcations at the stability transition of earthquake faulting. Geophys. Res. Lett. 47, e2020GL087985. https://doi.org/10.1029/2020GL087985.
Nath, S., Raj, A., Thingbaijam, K., Kumar, A., 2009. Ground motion synthesis and seismic scenario in Guwahati city—a stochastic approach. Seismol. Res. Lett. 80 (2), 233–242.
Ogata, Y., 2017. Statistics of earthquake activity: models and methods for earthquake predictability studies. Annu. Rev. Earth Planet. Sci. 45, 497–527. https://doi.org/10.1146/annurev-earth-063016-015918.
Palmer, T., 2019. Stochastic weather and climate models. Nat. Rev. Phys. 1 (7), 463–471.
Parzen, E., 2015. Stochastic Processes. Dover Edition, Courier Corporation.
Pathak, J., Hunt, B., Girvan, M., Lu, Z., Ott, E., 2018. Model-free prediction of large spatiotemporally chaotic systems from data: a reservoir computing approach. Phys. Rev. Lett. 120, 024102. https://doi.org/10.1103/PhysRevLett.120.024102.
Perfettini, H., Avouac, J.-P., 2004. Stress transfer and strain rate variations during the seismic cycle. J. Geophys. Res., Solid Earth 109, B06402. https://doi.org/10.1029/2003JB002917.
Perfettini, H., Molinari, A., 2017. A micromechanical model of rate and state friction: 1. Static and dynamic sliding. J. Geophys. Res., Solid Earth 122, 2590–2637. https://doi.org/10.1002/2016JB013302.
Pintori, F., Serpelloni, E., Longuevergne, L., Garcia, A., Faenza, L., D'Alberto, L., Gualandi, A., Belardinelli, M., 2021. Mechanical response of shallow crust to groundwater storage variations: inferences from deformation and seismic observations in the eastern southern Alps, Italy. J. Geophys. Res., Solid Earth 126 (2). https://doi.org/10.1029/2020JB020586.
Radiguet, M., Perfettini, H., Cotte, N., Gualandi, A., Valette, B., Kostoglodov, V., Lhomme, T., Walpersdorf, A., Cabral Cano, E., Campillo, M., 2016. Triggering of the 2014 m_w7.3 Papanoa earthquake by a slow slip event in Guerrero, Mexico. Nat. Geosci. 9. https://doi.org/10.1038/NGEO2817.
Rice, J., 1993. Spatio-temporal complexity of slip on a fault. J. Geophys. Res. 98 (B6), 9885–9907.
Rice, J., Ruina, L., 1983. Stability of steady frictional slipping. J. Appl. Mech. 50, 343–349.
Romanet, P., Bhat, H., Jolivet, R., Madariaga, R., 2018. Fast and slow slip events emerge due to fault geometrical complexity. Geophys. Res. Lett. 45, 4809–4819. https://doi.org/10.1029/2018GL077579.
Rubinstein, J., La Rocca, M., Vidale, J., Creager, K., Wech, A., 2008. Tidal modulation of nonvolcanic tremor. Science 319 (5860), 186–189. https://doi.org/10.1126/science.1150558.
Ruina, L., 1983. Slip instability and state variable friction laws. J. Geophys. Res. 88 (B12), 10359–10370.
Sano, M., Sawada, Y., 1985. Measurement of the Lyapunov spectrum from a chaotic time series. Phys. Rev. Lett. 55 (10), 1082–1085.
Sauer, T., Yorke, J., Casdagli, M., 1991. Embedology. J. Stat. Phys. 65 (3/4).
Scholz, C., 2019. The Mechanics of Earthquakes and Faulting, 3rd edition. Cambridge University Press.
Scott, D., Marone, C., Sammis, C., 1994. The apparent friction of granular fault gouge in sheared layers. J. Geophys. Res. 99 (B4), 7231–7246.
Scuderi, M., Marone, C., Tinti, E., Di Stefano, G., Collettini, C., 2016. Precursory changes in seismic velocity for the spectrum of earthquake failure modes. Nat. Geosci. 9. https://doi.org/10.1038/NGEO2775.
Segall, P., Rice, J., 1995. Dilatancy, compaction, and slip instability of a fluid-infiltrated fault. J. Geophys. Res. 100 (B11), 22155–22171.
Strogatz, S., 1994. Nonlinear Dynamics and Chaos, 1st edition. Perseus Books.
Takens, F., 1981. Detecting Strange Attractors in Turbulence, 2nd edition. Lecture Notes in Mathematics. Springer, p. 366.
Terzaghi, K., 1925. Erdbaumechanik auf bodenphysikalischer grundlage. F. Deuticke, Wien.
Theiler, J., 1990. Estimating the fractal dimension of chaotic time series. Linc. Lab. J. 3 (1).
Tinti, E., Scuderi, M., Scognamiglio, L., Di Stefano, G., Marone, C., Collettini, C., 2016. On the evolution of elastic properties during laboratory stick-slip experiments spanning the transition from slow slip to dynamic rupture. J. Geophys. Res., Solid Earth 121, 8569–8594. https://doi.org/10.1002/2016JB013545.
Vere-Jones, D., Ben-Zion, Y., Zúñiga, R., 2005. Statistical seismology. Pure Appl. Geophys. 162, 1023–1026. https://doi.org/10.1007/s00024-004-2659-2.
Wales, D., 1991. Calculating the rate of loss of information from chaotic time series by forecasting. Nature 350, 485–488.
Wolf, A., Swift, J., Swinney, H., Vastano, J., 1985. Determining Lyapunov exponents from a time series. Phys. D: Nonlinear Phenom. 16 (3), 285–317. https://doi.org/10.1016/0167-2789(85)90011-9.